

Persistent effects of a severe drought on Amazonian forest canopy

Sassan Saatchi^{a,b,1}, Salvi Asefi-Najafabady^b, Yadvinder Malhi^c, Luiz E. O. C. Aragão^d, Liana O. Anderson^{c,e}, Ranga B. Myneni^f, and Ramakrishna Nemani^g

^aJet Propulsion Laboratory, California Institute of Technology, Pasadena, CA 91109; ^bInstitute of Environment, University of California, Los Angeles, CA 90045; ^cEnvironmental Change Institute, School of Geography and the Environment, University of Oxford, Oxford OX1 3QY, United Kingdom; ^dCollege of Life and Environmental Sciences, University of Exeter, Devon EX4 4RJ, United Kingdom; ^eRemote Sensing Division, National Institute for Space Research (INPE), Sao Jose dos Campos, Sao Paulo 12227-010, Brazil; ^fDepartment of Geography and Environment, Boston University, Boston, MA 02215; and ^gBiospheric Sciences Branch, National Aeronautics and Space Administration/Ames Research Center, Moffett Field, CA 94035

Edited by Steven C. Wofsy, Harvard University, Cambridge, MA, and approved November 12, 2012 (received for review March 19, 2012)

Recent Amazonian droughts have drawn attention to the vulnerability of tropical forests to climate perturbations. Satellite and in situ observations have shown an increase in fire occurrence during drought years and tree mortality following severe droughts, but to date there has been no assessment of long-term impacts of these droughts across landscapes in Amazonia. Here, we use satellite microwave observations of rainfall and canopy backscatter to show that more than 70 million hectares of forest in western Amazonia experienced a strong water deficit during the dry season of 2005 and a closely corresponding decline in canopy structure and moisture. Remarkably, and despite the gradual recovery in total rainfall in subsequent years, the decrease in canopy backscatter persisted until the next major drought, in 2010. The decline in backscatter is attributed to changes in structure and water content associated with the forest upper canopy. The persistence of low backscatter supports the slow recovery (>4 y) of forest canopy structure after the severe drought in 2005. The result suggests that the occurrence of droughts in Amazonia at 5–10 y frequency may lead to persistent alteration of the forest canopy.

radar | canopy water content | rainforest | QSCAT | canopy disturbance

In the past decade, Amazonia has experienced two major droughts, as highlighted by the water level of the Rio Negro recorded at Manaus in central Amazonia, the longest (109 y) available time series record. The first occurred in 2005 (1, 2), with the minimum river level at 14.75 m, the lowest in the past 40 y, and the second in 2010, with the river at 13.63 m, the lowest in the record (3). Severe droughts, often associated with the El Niño–Southern Oscillation (ENSO), cause a decline in soil moisture, pushing the plant-available water below a critical threshold level for a prolonged period, resulting in higher rates of tree mortality and increased forest flammability (4–7). The drought of 2005 was unlike the ENSO-related droughts because of its temporal and spatial extent: its peak of intensity during the dry season and its center of impact in southwestern Amazonia, rather than the central and eastern regions, which are associated more with El Niño droughts (1).

Warming of the tropical North Atlantic sea surface temperature is considered a major contributing factor in the 2005 drought, which resulted in the lowest river levels recorded to that date in southern and western tributaries (1, 8, 9). Observations from ground stations show that precipitation over the southern region of Amazonia declined by almost 3.2% per year in the period before this decade (1970–1998) (10). The same region experienced several negative precipitation anomalies during the last decade, indicating an increase in dry conditions that culminated in severe 2005 drought (1–3, 11). Climate model predictions also suggest that the intensity of dry seasons and extreme dry events may increase with climate change, affecting the ecosystem function and health of forests in Amazonia (11, 12).

The short-term consequences of drought events are well established through ground and satellite observations (3–6, 13). However, the extent and severity of longer-term impacts of droughts on

the Amazonian rainforest and its functioning are not known. Measurements of forest structure and density from inventory plots over humid tropical forests have shown an increase in tree mortality and a decline in the aboveground biomass that may persist for several years (4, 14, 15). A relationship found between a simple measure of moisture stress and changes in forest biomass was used recently to predict the potential impacts of droughts on the Amazon carbon dynamics (6). Direct evidence of long-term impacts of droughts on the Amazon vegetation has been demonstrated only in controlled small-scale (1-ha plot) field experiments (16). The study showed the most important forest response to severe droughts was the mortality of large trees with crowns in the upper canopy when plant-available soil water declined below a critical threshold (16, 17). Similar drought effects have been observed in Amazonia and other regions in research plots (4, 18).

Sensitivity of satellite spectral observations to the forest's upper-canopy characteristics (greenness, leaf area), particularly at optical wavelengths, potentially may provide the necessary information to assess the long-term impacts of droughts (18). However, recent results from optical satellites monitoring changes in vegetation greenness after the 2005 drought have been contradictory because of severe impacts of clouds and atmospheric aerosols on spectral observations (3, 19–22) over Amazonia. No study has examined the potential changes of vegetation detectable at microwave frequencies.

Here, we analyze data from two microwave satellite sensors measuring precipitation and canopy water content to quantify the relative severity of recent droughts and potential impacts on Amazonian vegetation (*Methods*). First, we characterize the drought over Amazonia by calculating three indices derived from monthly precipitation measured by the Tropical Rainfall Measuring Mission (TRMM; 1998–2010): the dry-season precipitation anomaly (DPA), dry season water deficit anomaly (DWDA), and maximum climatological water deficit (MCWD) (*SI Methods*). These indices are complementary in their information content and provide spatially specific indicators about the extent and severity of moisture deficit in Amazonia.

Second, we examine the impact of the water deficit on the Amazon forest by using observations from the SeaWinds Scatterometer onboard QuickSCAT (QSCAT: 2000–2009). QSCAT operates in microwave frequency (13.4 GHz), providing backscatter measurements strongly affected by the temporal and spatial variations of water content and structure of the forest canopy (*Fig. S1*) (13, 22).

Author contributions: S.S., L.E.O.C.A., R.B.M., and R.N. designed research; S.S., S.A.-N., and L.O.A. performed research; S.S., Y.M., L.E.O.C.A., R.B.M., and R.N. contributed new reagents/analytic tools; S.S. and S.A.-N. analyzed data; and S.S. and Y.M. wrote the paper.

The authors declare no conflict of interest.

This article is a PNAS Direct Submission.

¹To whom correspondence should be addressed. E-mail: saatchi@jpl.nasa.gov.

This article contains supporting information online at www.pnas.org/lookup/suppl/doi:10.1073/pnas.1204651110/-DCSupplemental.

QSCAT signal propagating at 2.1-cm wavelength and incidence angles of about 50° penetrates a few meters (1–5 m) into the forest canopy, depending on forest gaps, and scatters from leaves and branches of the upper canopy of trees. The backscatter measurements capture biophysical properties of forests, such as the water content in leaves and branches, and canopy structure (i.e., volume or biomass) (*SI Materials and Methods*). Temporal changes (diurnal and seasonal) of canopy water content (i.e., leaves and branches) and seasonal leaf phenology have the largest impact on the radar backscatter (23). Structural changes such as large-scale forest degradation and deforestation that may change the canopy roughness (layering of tree crowns), create gaps, and affect the water content or biomass of the upper canopy of forests can change the backscatter signal significantly (Fig. S1). However, because of the incidence angle and large footprint of QSCAT radar, other factors, such as soil moisture and variations in leaf clumping or orientation of branches, have less impact on the QSCAT backscatter (23).

In November 2009, QSCAT sensor scanning capability failed and the sensor stopped collecting systematic data globally, limiting our analysis of the changes in canopy characteristics when the 2010 drought occurred. However, before its scanning failure, throughout its mission (1999–2009) QSCAT provided reliable data over ocean and land surface without any bias or sensor degradation and continued providing limited data along its orbital passes (*SI Materials and Methods*). To examine the impact of the 2010 drought, we analyzed TRMM precipitation radar (TRMM-PR) backscatter data operating at the same frequency as QSCAT but with nadir-looking incidence angle and surface backscatter measurements for periods of no rain. TRMM-PR backscatter responds to the surface moisture by penetrating deeper into the canopy and scattering from soil and understory vegetation through forest gaps (*SI Materials and Methods*).

We used time series of QSCAT backscatter data from dawn orbits to monitor vegetation in its least-stressed time of day by studying its monthly and seasonal normalized anomaly and spatial variations over Amazonia. Throughout the time-series analysis, the QSCAT backscatter measurement was used as a direct representation of the upper-canopy forest structure and water content to avoid any indirect estimation and validation of water content or structure (13).

Results

Patterns of Water Deficit. The three indices derived from TRMM data show a strong negative anomaly over southwestern Amazonia in 2005 (Fig. S2). Of the total current forested area of the Amazon basin ($\sim 5.5 \text{ M/km}^2$), about 30% (1.7 M/km^2) experienced standardized DWDA less than -1.0σ (σ : SD) in 2005, and more than 5% of total area (0.27 M/km^2) was subject to severe anomalies (DWDA less than -2.0σ). Both the spatial extent and the severity of drought increased in 2010, resulting in more than 48% (2.6 M/km^2) of the forest area subject to DWDA less than -1.0σ , and about 20% (1.1 M/km^2) at DWDA less than -2.0σ (Fig. S2). In south and southwestern regions of Amazonia, this anomaly was superimposed on a dry season that is fairly strong in normal years, resulting in the forests experiencing a very large water deficit (MCWD less than -300 mm) by the end of the dry season. The generally wetter forests in central Amazonia with the largest negative DPA and DWDA experienced low to moderate water deficit (MCWD less than -100 mm) in 2005 and 2010. Data show that precipitation anomalies over these regions lasted only over a relatively short time span within the last decade. However, the spatial extent of precipitation anomaly (DPA) and MCWD in southwestern Amazonia reached to the foothills of the Andes in 2005 and extended to northern regions of Peru, Ecuador, and Colombia, suggesting a pattern approximately consistent with the low river stage measured in Rio Negro and other rivers in the southwestern Amazon basin (2, 9).

Patterns of Drought Impact on Forest Canopy. The impact of this extensive water deficit on the Amazon forest was captured by the QSCAT (2000–2009) backscatter time series (*SI Materials and Methods*). The dry season standardized anomaly in 2005 showed widespread (2.1 M/km^2) decline in forest canopy backscatter (anomaly less than -1.0σ) in southwestern Amazonia (Fig. 1A). Nearly 40% of this area (0.77 M/km^2) indicated a major decline in backscatter (anomaly less than -2.0σ). The backscatter anomaly on a monthly or seasonal basis calculated for 2000–2009 shows a strong spatial correlation with the water deficit anomaly (WDA) observed by TRMM for the same period, indicating that water stress is the likely cause of the change in forest canopy properties. The region affected by the QSCAT anomaly covered a variety of old-growth forests, from transitional semideciduous and bamboo forests in southwestern Brazil, northern Bolivia, and areas in southern Peru and along the Andean flank in western Amazonia to a variety of inundated and *terra firme* forests in the north (24). All nonforested areas were excluded from the analysis using a global land cover type (*SI Materials and Methods*).

We performed cross-correlation between the QSCAT and TRMM anomaly averaged over Amazonia and found correlation was significant with 1–3 mo lag, but varied over the basin depending on the rainfall patterns (Fig. 1B and C). In the southwestern region, with a longer dry season, the correlation was lagged significantly by about 3 mo. However, in the northeastern region, where the dry season is moderate and short, the correlation was strong, with no time lag. Spatial variations of QSCAT and TRMM anomaly in 2005 show that areas captured by highly negative QSCAT anomaly (less than -3.0σ) are larger in extent than similar areas captured by WDA. The difference is explained by closely examining areas where maximum water deficit (MCWD) in 2005 exceeded 300 mm and/or there was a strong water deficit during the entire driest quarter (DWDA less than -3.0σ). The reduction in QSCAT backscatter, causing the anomaly in the southwest region, is closely associated with the WDA gradually developing through the dry season in 2005 (Fig. S3).

Slow Recovery of Forest Canopy. We used the time series of TRMM and QSCAT anomaly averaged over the area affected by the drought in southwestern Amazonia (4°S – 12°S , 76°W – 66°W) to examine the temporal patterns of the 2005 drought and its impacts. After 2005, the area affected by the drought had a recovery of total rainfall, but WDA stayed negative on the average during the 2006 and 2007 dry seasons. Recovery of water deficit started in 2008 followed by an anomalously wet year in 2009 that extended over all of Amazonia except the northeastern region (Fig. S4). From late 2009, the water deficit increased before it rapidly reached its highest value in the decade in southwestern region (Fig. 2A). However, most remarkably, forest pixels affected by the water deficit over southwestern Amazonia continued to show low values in the QSCAT backscatter (about 20% below previous mean) from 2005 through to the end of the record in November 2009 (Fig. 2B). We used an autoregressive moving-average (ARMA) model with an order of about 5% of the data points ($>6 \text{ mo}$) to highlight the longer-term trends and cycles in the data. The time series of the QSCAT anomaly suggests that the 2005 drought caused a step change in the backscatter properties of the canopy, with little recovery in the subsequent years (*SI Materials and Methods*). The response is very localized to regions in western Amazonia that experienced the strongest water deficit anomalies, hence cannot be attributed to hypothetical changes in sensor performance. We tested the sensor performance in other regions of Amazonia and the world to ensure the stability of the backscatter signal and its calibration (Fig. S5). Spatial patterns of annual QSCAT anomaly for the dry season support the long-term reduction in backscatter after the 2005 drought until the end of 2009, when the positive anomaly of

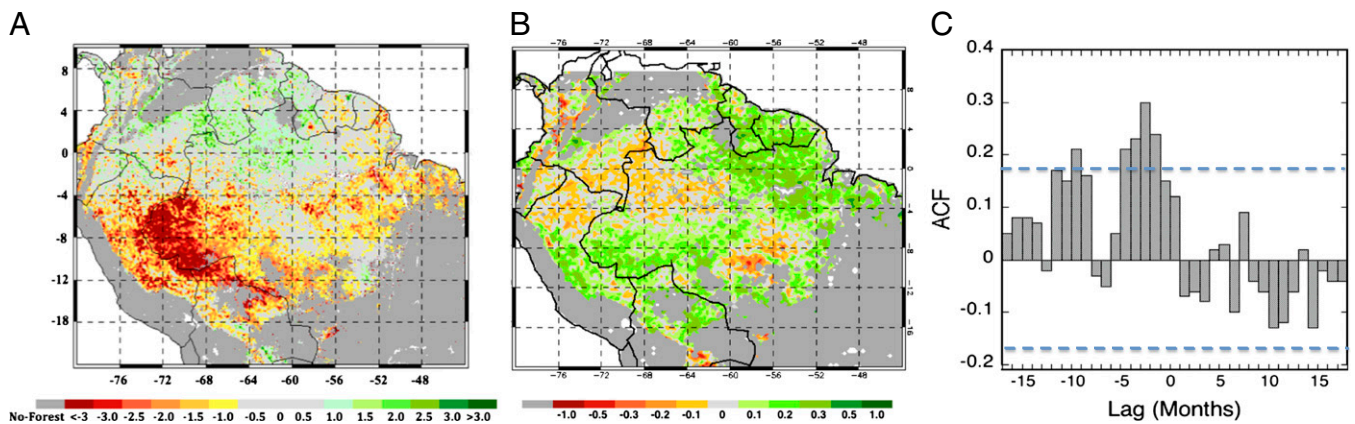


Fig. 1. Spatial extent and severity of the 2005 Amazonian drought using seasonal (JAS) standardized anomaly of QSCAT backscatter data at H polarization for ascending orbits (acquired at dawn), capturing the forest canopy water stress and spatial patterns. (A) Magnitudes of QSCAT anomaly beyond $\pm 1.0 \sigma$. (B) Spatial cross-correlation between the TRMM monthly WDA and the QSCAT monthly anomaly with 1 mo lag over the period 2000–2009. (C) ACF developed between the two datasets averaged over forested pixels in Amazonia with time lags ranging from 0 to 18 mo in either direction. Dashed lines represent the 95% confidence interval as $\pm 2/\sqrt{N}$.

precipitation slightly changed the trend before the 2010 drought (Fig. S5).

The intensity of the anomaly in 2005 and its gradual shift toward recovery lagging the water deficit also is evident in the distributions of normalized anomalies for the dry season water deficit and the canopy backscatter power over pixels in southwestern Amazonia (Fig. S6). The distribution of the QSCAT anomaly peaked at a value between -2 and -2.5σ but stayed significantly negative and different from the distribution of the entire time series for years before 2005 that peaked at about zero ($P < 0.01$ from a two-sided t test). During this period, the distribution of water deficit over the same region alternated between negative and positive, with a strong negative in 2005

(approximately -1.5σ), relatively significant water deficit anomalies in summer of 2006 and 2007 (approximately -1.2σ), and a strong anomaly in 2010 (peaked between -1.5 and -2.0σ).

The variation of QSCAT anomaly before and after the 2005 drought was tested through statistical time-series analysis to quantify significance of the step change and trends in the data (*SI Materials and Methods*). Using an ARMA analysis over 120 mo (2000–2009), we found that the QSCAT time series was piecewise stationary because of changes in the mean and, to some extent, the variance over time caused by the 2005 drought. The autocorrelation function (ACF) and partial ACF (PACF) suggested that the time series had a lag of 1–3 mo with PACF cutoff after lag 1 (95% confidence interval), allowing the process to be represented by autoregressive (AR) model (1) on the monthly but not annual time scale (Fig. S7). The detection of the step change in the QSCAT time series was performed using the Breaks in Additive Season and Trend (BFAST) algorithm based on the iterative decomposition of time-series data (25). The results show that a significant step change in QSCAT data was detected in June 2005 with root-mean-square error (RMSE) of 1 mo under the assumption of 97.5% (3σ) of the noise range in the data (Fig. 3). The noise level did not influence the RMSE of the detection, indicating a low commission error in the detection performance (*SI Materials and Methods*). The BFAST algorithm also detected the seasonality of QSCAT anomaly and showed that it did not influence the accuracy of detecting the breakpoint in the time-series data. The post-2005 trend in the time series was not significant, although it showed the slow recovery of QSCAT signal that lasted about 4 y after the 2005 drought (Fig. 3).

To demonstrate the changes in QSCAT signal relative to TRMM water deficit, we used the average monthly normalized anomalies for southwestern Amazonia and calculated the relative difference between QSCAT anomaly and TRMM monthly WDA (both are normalized and unitless). On average, the difference in anomalies stayed at zero (zero slope) before the 2005 drought and had a negative slope after 2005, suggesting a lag in recovery of QSCAT anomaly relative to the TRMM WDA in southwestern Amazonia. The largest decline in QSCAT backscatter occurred in September 2005 from gradual development of negative anomalies during the driest quarter in July, August, and September (JAS). We extended the analysis over the entire Amazonia by mapping the spatial distribution of the pixels with negative anomalies in both QSCAT and TRMM data (less than -1.0σ) and with significantly ($P < 0.01$) negative slopes (*SI Materials and Methods*) between QSCAT anomaly and WDA

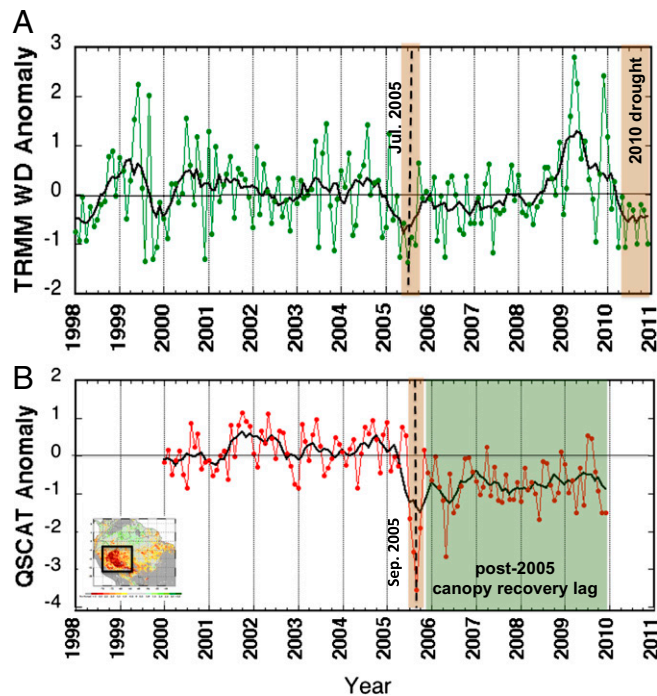


Fig. 2. Time series of (A) TRMM and (B) QSCAT monthly anomaly over western Amazonia (window: 4°S – 12°S , 76°W – 66°W). Solid lines show the result of the ARMA of the order of 6 mo.

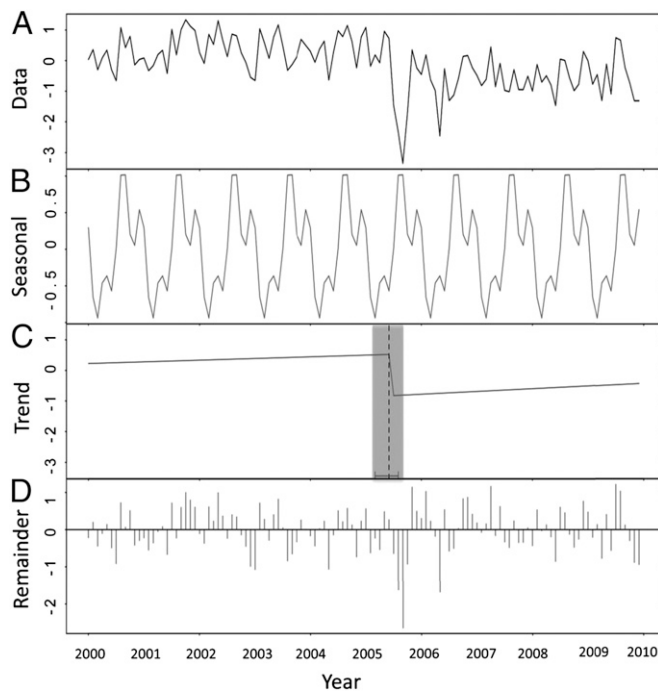


Fig. 3. (A) BFAST seasonal trend decomposition of the QSCAT monthly normalized anomaly time series of southwestern Amazonia (window: 4°S–12°S, 76°W–66°W) into seasonal, trend, and remainder components. (B) The seasonal component is estimated by taking the mean of all seasonal sub-components starting from January 2000. The range of seasonal amplitude is less than 20% of the range of QSCAT anomaly. (C) One abrupt change in the trend component of the time series is detected on June 2005. The shaded bar indicates the 97.5% (3σ) confidence interval. (D) The remainder shows the variation of the signal after the removal of the trend capturing the temporal variations in the time series.

after the 2005 drought (Fig. 4A). Pixels with larger negative slopes represent areas with a longer lag in canopy recovery relative to the recovery of the water deficit and showing persistent drought impacts on canopy characteristics. Regions A and B, respectively, show the old-growth forests of southern Peru and the states of Acre and Rondônia in the western Amazon of Brazil. Region C covers a mosaic of undisturbed and disturbed forests in the state of Mato Grosso and southern Pará (both in Brazil). All three regions were reported to have an anomalously higher number of fires in 2005 and subsequent years, suggesting a potential lower canopy water content and higher fuel loads (4, 22). The 2005–2009 forest loss and degradation from deforestation and fire impacts did not change the persistent QSCAT negative anomaly (Fig. S8). However, a significantly large number of fires during 2005–2009 (>35%) occurred in QSCAT pixels with strong negative anomaly (less than -1.0σ) in 2005, and more than 78% of fires in 2010 occurred in pixels with large negative slopes (less than -0.01). The occurrence of fires and the areas with slow recovery after the drought coincided with regions with large seasonality of backscatter in QSCAT data, pointing predominantly to transitional and seasonal forests of Amazonia (Fig. 4B) (SI Materials and Methods).

Discussion

Overall, the results of QSCAT analysis indicate two important conclusions. First, the QSCAT anomaly captures the extent and intensity of the 2005 drought impact on the Amazon forest and provides patterns consistent with areas that experienced the largest water deficit in the driest quarter. Changes in QSCAT backscatter are the result of changes in the properties of the top

layer of the canopy, consisting of emergent crowns that often are exposed to higher vapor-pressure deficits and consequently are more sensitive to droughts (4, 16). Theoretically, the widespread decline in radar backscatter suggests changes in canopy water content and structure (e.g., fresh biomass), unlike what was observed in optical sensing (3, 20). The decline in backscatter suggests a reduction of upper-canopy biomass or canopy roughness attributed to potential drought-driven disturbance. The magnitude of the decline in 2005 is significantly larger than seasonal amplitude of the QSCAT backscatter caused by phenology and changes of canopy water content from natural cycles of dry and wet seasons.

Second, the QSCAT anomaly remained negative after the 2005 drought over a large area in western Amazonia, suggesting the persistent effect of the drought on the forest canopy. The severity of the disturbance caused a slow recovery of the forest canopy to its predrought condition in terms of biomass or roughness (canopy layering), lagging the precipitation recovery of subsequent years until the 2010 drought. Notably, more than 0.6×10^6 km² of areas affected by the 2005 drought (QSCAT anomaly less than -2.0σ) coincided with the areas affected by the 2010 water deficit (TRMM DWDA less than -2.0σ), suggesting a potentially widespread exacerbation of stress on forests of south and western Amazonia.

Without extensive surveys and perhaps airborne observations and validations, the interpretation of the decline of backscatter and its direct relation to the forest disturbance remain challenging. A simple wilting or shedding of leaves during the peak drought, resulting in a temporary decline of net primary production, would be expected to be followed by recovery of canopy properties within a year. Such recovery is apparent in central Amazonia, where the backscatter anomaly recovered rapidly, despite experiencing a strong water deficit and QSCAT anomaly in 2005 (Figs. S2 and S3). The delayed recovery of QSCAT in southwestern Amazonia suggests a decline in more long-lived aspects of canopy structure with recovery timescales greater than 3–4 y, such as loss of leaves or dieback of branches, or potential tree falls creating large gaps.

We found no in situ observations over the region affected by the 2005 drought that could be used to directly verify our results. However, in most tropical drought studies, there is strong evidence that large-diameter or emergent trees have significantly higher mortality than small trees (16–18, 26, 27). The effects of extreme droughts on the understory light environment of tropical forests may be compared with the effects of tree-fall gaps, although on much larger scales (27). With the recovery of rainfall and potential increase in light availability due to gaps from canopy disturbance, the understory vegetation and pioneer species may increase productivity a few months after severe droughts (22). These changes may affect nadir-looking optical satellite observations with sensitivity to vegetation greenness and photosynthesis capacity (3, 21, 22). In situ measurements show that the mortality of large trees remains elevated even a few years after the drought (4), suggesting a decline in canopy structure or biomass followed by gradual development of canopy emergent trees (4, 22). The recovery of canopy trees after the drought event is a slower process and may take longer to reach the predrought state (18, 22, 25, 26). Based on the results from this study and the evidence reported in the literature, we hypothesize that western Amazonia experienced a large-scale canopy disturbance from the 2005 drought, resulting in the decline of emergent and canopy tree structure and biomass that continued with a slow recovery for the next few years. We expect future field campaigns directed to examine the effect of severe droughts and analysis of existing in situ data from permanent research plots in western Amazonia (4) to test the hypothesis and potentially verify the results of satellite observations.

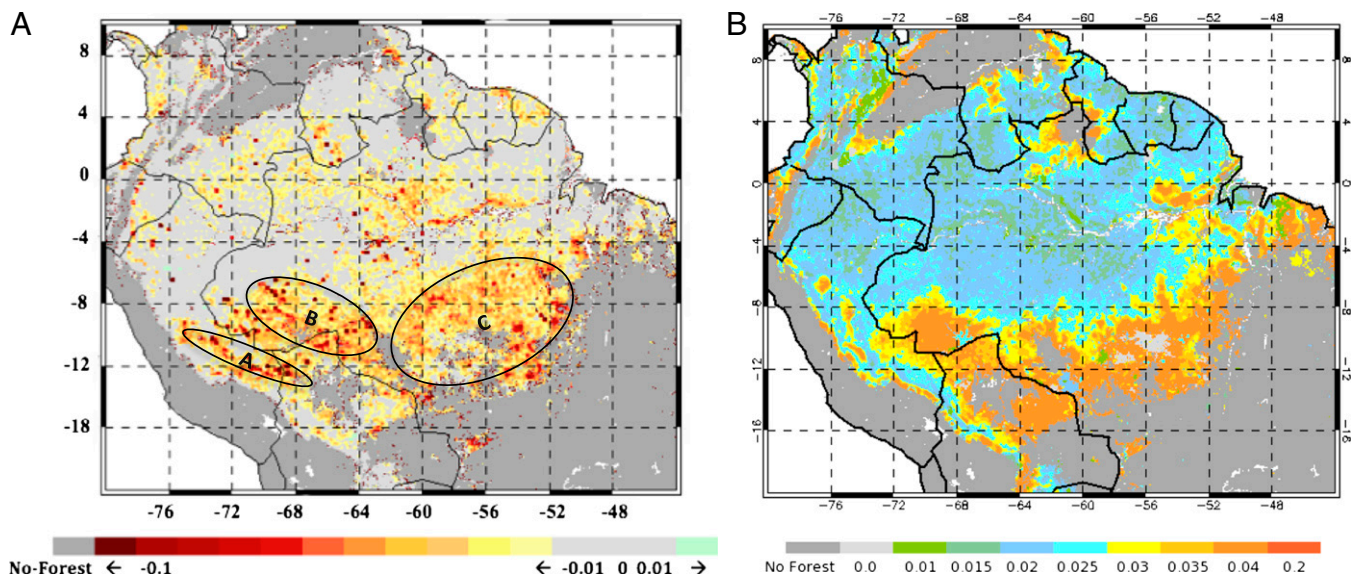


Fig. 4. (A) Spatial representation of the rate of recovery of pixels affected by QSCAT-negative anomaly (less than -1.0σ) calculated by the slope of the difference in QSCAT and TRMM monthly anomalies from September 2005 to November 2009 (*SI Materials and Methods*). Pixels with significantly large negative slopes represent forests with slower recovery and cover an area of $\sim 4 \times 10^5 \text{ km}^2$. Areas delineated in highlighted areas as A, B, and C represent regions in southeastern Peru, the state of Acre in Brazil, and areas in the state of Mato Grosso, respectively, showing areas with potentially the largest impacts of the 2005 drought. (B) Spatial representation of areas with strongest seasonality in canopy properties detected by the QSCAT backscatter measurements (2000–2009).

A large-scale drought disturbance of forest structure from mortality of large trees and, to some extent, a drop in the leaf area of the forest (16, 28) may lead to a sustained efflux of carbon dioxide from the decay of wood, with the process significantly perturbing the net ecosystem exchange and carbon fluxes (11, 12, 14). Results from climate analysis for the period 1995–2005 demonstrate a steady decline in plant water availability over the same region, suggesting a decade of moderate water stress before the 2005 drought (10, 22), helping to trigger a large-scale canopy disturbance after the 2005 drought. A higher water deficit in subsequent years, together with another strong local drought in 2007, suggests that soils from a large portion of southwestern Amazonia may not have reached the field capacity, which would favor canopy recovery (29). Other factors, such as a decline in rainfall and larger variability in the dry season over southwestern Amazonia since the late 1980s and early 1990s (Fig. S9), may have contributed to an increasingly drier condition in this region. We show that these recent negative anomalies and year-to-year variations are strongly linked to both the warming and variations in the sea surface temperature (1, 2). The most recent droughts are related to higher temperatures in the tropical Atlantic, showing a strong regional sensitivity of WDA to the tropical North Atlantic index (Fig. S10).

Our analysis ends in 2009. It seems likely that the observed canopy response was repeated in the more severe drought of 2010 (Fig. S11), for which QSCAT data are not available; hence, a new wave of disturbance may have affected forest canopies not yet recovered from the previous droughts and water deficit. The TRMM-PR backscatter anomaly suggests that the surface moisture in western and southern Amazonia dropped significantly in 2010 and lasted longer than the dry season (Fig. S11), potentially causing more stress on the forest canopy. If droughts continue to occur at 5–10-y frequency, or increase in frequency, large areas of Amazonian forest canopy likely will be exposed to the persistent effect of droughts and the slow recovery of forest canopy structure and function. In particular, areas of south and western Amazonia have been shown to be affected severely by increasing rainfall variability in the past decade, suggesting that

this region may be witnessing the first signs of potential large-scale degradation of Amazonian rainforest from climate change (10, 11, 30).

Materials and Methods

This study is based on the use of various microwave satellite observations of Amazonia to detect the regional and potential severity of the impact of the 2005 drought on the Amazon forests. Our approach includes five steps: (i) spatial analysis of monthly TRMM rainfall data to calculate the standardized anomaly of rainfall during the dry season, maximum water deficit, and anomaly of monthly water deficit; (ii) spatial analysis of monthly QSCAT backscatter data to compute pixel-level standardized anomaly from the satellite dawn orbits to monitor vegetation in its least-stressed time of day and its spatial correlation with TRMM water deficit; (iii) time-series analysis of QSCAT monthly backscatter anomaly over western Amazonia using the ARMA model, testing ACF and PACF with time lags, and iterative application of the additive decomposition algorithm BFAST to detect a significant breakpoint and trend in the QSCAT data associated with the 2005 drought; (iv) quantifying the impact of deforestation and fire occurrence on the QSCAT anomaly and trend results and showing the independence of the results from canopy disturbances that may have been caused by fire and degradation during and after the 2005 drought; and (v) testing the regional impacts of variations in the historical climate data on the patterns of rainfall anomaly in Amazonia to explain the climatic cause of recent droughts in Amazonia. Our analysis of the QSCAT data was limited to the period 2000–2009 and could not provide information about the 2010 drought. We included the TRMM-PR backscatter anomaly to demonstrate the changes in surface moisture during the 2005 and 2010 droughts as evidence of the potential impact of the 2010 drought on forests in southwestern Amazonia already affected.

We used the Moderate Resolution Imaging Spectroradiometer (MODIS) land cover map of 2005, GlobCover land cover map of 2009, and MODIS-derived pixel fire counts from 2001 to 2010 to exclude nonforest pixels from our analysis and to quantify the percentage of pixels with a large QSCAT-negative anomaly affected by fires after the 2005 drought (2005–2009) and during the 2010 drought. We had no independent ground measurements to verify our results because of the large pixel size of the satellite observations and the recentness of the drought event. However, we provided biophysical interpretation of the satellite observations and evidence from *in situ* measurements and ecological studies to corroborate our findings of the persistent effect of droughts on forest canopy. We provide detailed information about the data in *SI Materials and Methods*.

ACKNOWLEDGMENTS. We thank Ryan Harrington from the University of California at Los Angeles (UCLA) Center for Tropical Research for his contribution in time-series analysis. The enhanced-resolution QSCAT data were produced by Prof. David Long at Brigham Young University as part of the National Aeronautics and Space Administration (NASA)-sponsored Scatterometer Climate Record Pathfinder. The precipitation data used in this study were acquired

as part of the TRMM project jointly sponsored by the Japan National Space Development Agency (NASDA) and NASA Office of Earth Sciences. The research was partially supported by NASA grants at the Jet Propulsion Laboratory and the UCLA Institute of Environment and by Natural Environment Research Council (London) Grants NE/F015356/2 and NE/I018123/1 at the University of Exeter and Grant NE/F005806/1 at the University of Oxford, United Kingdom.

1. Marengo JA, et al. (2008) The drought of Amazonia in 2005. *J Clim* 21:495–516.
2. Marengo JA, et al. (2011) The drought of 2010 in the context of historical droughts in the Amazon region. *Geophys Res Lett* 38:L12703 10.1029/2011GL047436.
3. Xu L, et al. (2011) Widespread decline in greenness of Amazonian vegetation due to the 2010 drought. *Geophys Res Lett* 38:L07402 10.1029/2011GL046824.
4. Phillips OL, et al. (2009) Drought sensitivity of the Amazon rainforest. *Science* 323(5919):1344–1347.
5. Aragão LEOC, et al. (2008) Interactions between rainfall, deforestation and fires during recent years in Brazilian Amazonia. *Philos Trans R Soc Lond B Biol Sci* 363(1498):1779–1785.
6. Lewis SL, Brando PM, Phillips OL, van der Heijden GM, Nepstad D (2011) The 2010 Amazon drought. *Science* 331(6017):554.
7. Nepstad D, et al. (2004) Amazon drought and its implications for forest flammability and tree growth: A basin-wide analysis. *Glob Change Biol* 10:704–717.
8. Davidson EA, et al. (2012) The Amazon basin in transition. *Nature* 481(7381):321–328.
9. Zeng N, et al. (2008) Causes and impacts of the 2005 Amazon drought. *Environ Res Lett* 3(1), 10.1088/1748-9326/3/1/014002.
10. Li W, Fu R, Juárez RI, Fernandes K (2008) Observed change of the standardized precipitation index, its potential cause and implications to future climate change in the Amazon region. *Philos Trans R Soc Lond B Biol Sci* 363(1498):1767–1772.
11. Malhi Y, et al. (2009) Exploring the likelihood and mechanism of a climate-change-induced dieback of the Amazon rainforest. *Proc Natl Acad Sci USA* 106(49):20610–20615.
12. Cox PM, et al. (2008) Increasing risk of Amazonian drought due to decreasing aerosol pollution. *Nature* 453(7192):212–215.
13. Frolking S, et al. (2010) Tropical forest backscatter anomaly evident in SeaWinds scatterometer morning overpass data during 2005 drought in Amazonia. *Remote Sens Environ* 115:897–907.
14. Phillips OL, et al. (2010) Drought-mortality relationships for tropical forests. *New Phytol* 187(3):631–646.
15. Williamson GB, et al. (2000) Amazonian tree mortality during the 1997 El Niño drought. *Conserv Biol* 14:1538–1542.
16. Nepstad DC, Tohver IM, Ray D, Moutinho P, Cardinot G (2007) Mortality of large trees and lianas following experimental drought in an Amazon forest. *Ecology* 88(9):2259–2269.
17. da Costa ACL, et al. (2010) Effect of 7 yr of experimental drought on vegetation dynamics and biomass storage of an eastern Amazonian rainforest. *New Phytol* 187(3):579–591.
18. Nakagawa M, et al. (2000) Impact of severe drought associated with the 1997–1998 El Niño in a tropical forest in Sarawak. *J Trop Ecol* 16:355–367.
19. Asner GP, Alencar A (2010) Drought impacts on the Amazon forest: The remote sensing perspective. *New Phytol* 187(3):569–578.
20. Saleska SR, Didan K, Huete AR, da Rocha HR (2007) Amazon forests green-up during 2005 drought. *Science* 318(5850):612.
21. Samanta A, et al. (2010) Amazon forests did not green-up during the 2005 drought. *Geophys Res Lett* 37:L05401–L05406.
22. Anderson LO, et al. (2010) Remote sensing detection of droughts in Amazonian forest canopies. *New Phytol* 187(3):733–750.
23. Frolking S, et al. (2006) Evaluation of the SeaWinds scatterometer for regional monitoring of vegetation phenology. *J Geophys Res* 111, 10.29/2005JD006588.
24. Pires JM, Prance GT (1985) The vegetation types of the Brazilian Amazon. *Key Environments: Amazonia*, eds Prance GT, Lovejoy TE (Pergamon, New York), pp 109–145.
25. Verbesselt J, Hyndman R, Zeileis A, Culvenor D (2010) Phenological change detection while accounting for abrupt and gradual trends in satellite image time series. *Remote Sens Environ* 114:2970–2980.
26. Condit R, Hubble SP, Foster RB (1995) Mortality rates of 205 neotropical tree and shrub species and the impact of a severe drought. *Ecol Monogr* 65:419–439.
27. Slik JW (2004) El Niño droughts and their effects on tree species composition and diversity in tropical rain forests. *Oecologia* 141(1):114–120.
28. Brando PM, et al. (2010) Seasonal and interannual variability of climate and vegetation indices across the Amazon. *Proc Natl Acad Sci USA* 107(33):14685–14690, 10.1073/pnas.0908741107.
29. Meir P, et al. (2009) The effects of drought on Amazonian rainforests. *Amazonia and Global Change*, Geophysical Monograph Series, ed Keller M, et al. (American Geophysical Union, Washington, DC), Vol 186, pp 429–449.
30. Zelazowski P, Malhi Y, Huntingford C, Sitch S, Fisher JB (2011) Changes in the potential distribution of humid tropical forests on a warmer planet. *Philos Transact A Math Phys Eng Sci* 369(1934):137–160.

Supporting Information

Saatchi et al. 10.1073/pnas.1204651110

SI Materials and Methods

Tropical Rainfall Measuring Mission Data Analysis. Monthly time series (1998–2010) of Tropical Rainfall Measuring Mission (TRMM)-merged precipitation data at 0.25° spatial resolution (3B43-v6: Goddard Distributed Active Archive Center (GES DISK DAAC) with cumulative values estimated in millimeters per month were used to calculate the monthly precipitation anomaly and dry-season [July, August, and September (JAS)] precipitation anomaly (DPA) of 2005 and 2010 (Fig. S2). The anomaly on a pixel-by-pixel basis (i, j) for each year (y) was calculated as a departure from the 1998–2010 mean ($TRMM_{1998-2010}$), excluding the measurement from year (y) and normalized by the standard deviation (STD):

$$TRMM_y \text{ anomaly}(i, j) = \frac{TRMM_y(i, j) - \langle TRMM_{1998-2010}(i, j) \rangle}{STD(TRMM_{1998-2010}(i, j))}$$

As a complementary measure of drought, we also calculated the monthly water deficit (WD) and cumulative WD (CWD) values at the pixel level from the TRMM time series. For this, we first calculated the monthly WDs based on the approximation that a moist tropical canopy transpires about 100 mm/mo. This value was obtained from ground measurements in different locations and seasons in Amazonia (1). If the monthly precipitation is less than 100 mm, the forest enters WD; otherwise, the WD is set to zero. First, we calculate WD for each month (n) from (2):

$$\begin{aligned} &\text{if } WD_{n-1}(i, j) - E(i, j) + TRMM_n(i, j) < 0, \\ &\text{then } WD_n(i, j) = WD_{n-1}(i, j) - E(i, j) + TRMM_n(i, j), \\ &\text{else } WD_n(i, j) = 0 \end{aligned}$$

where $E(i, j)$ is the evapotranspiration and $TRMM_n(i, j)$ is the monthly precipitation at each pixel. The WD as calculated in the above equation is the same as the CWD of any month representing the sum of WD values up to and including that month (3); the maximum climatological WD (MCWD) in a year is the maximum value of CWD recorded in that year. The WD will always reset to zero when monthly rainfall is greater than 100 mm. This will allow a relatively wet dry season to have no impact on the maximum WD. The seasonal WD is obtained by implementing the above formula for every quarter and using the WD from July to September as the WD for the dry season.

We used the DPA, dry-season WD anomaly (DWD), and MCWD as three measures to map the extent and intensity of droughts. Together, these measures are strong predictors of drought intensity and provide complementary spatial information on the extent of droughts that correlate with tree mortality. DPA and DWD for 2005 and 2010 show the patterns of anomalous water availability extending from southwestern Amazonia to the interior of the basin, where forests do not often experience a dry season in normal years (Fig. S2). However, MCWD provides the magnitude of WD related to the intensity of drought and its spatial footprint in south and southwestern Amazonia.

QuickSCAT Data Analysis. The entire record of QuickSCAT (QSCAT) time-series data (1999–2009) was obtained from the National Aeronautics and Space Administration (NASA) Scatterometer Climate Record Pathfinder (www.scp.byu.edu/). The dataset contains the enhanced resolution (4.45-km pixel grid and 8–9-km effective resolution) four-dimensional (4D) composites at both H (horizontal) and V (vertical) polarizations and for

ascending and descending orbits with equator crossing at 0600 and 1800 hours local standard time (LST), respectively. We chose QSCAT as an alternative to optical Moderate Resolution Imaging Spectroradiometer (MODIS) data to study the Amazon vegetation response to droughts (4) because (i) the radar backscatter at microwave frequency (13.4 GHz) and high incidence angle ($\sim 46^\circ$ and 54° from zenith) over dense forest cover is strongly sensitive to the upper-canopy (predominately leaf and branch) structure and water content through the canopy dielectric properties (Fig. S1) (5, 6), and (ii) being an active microwave sensor, QSCAT images over tropical forests have almost no effects from the presence of clouds and aerosols, and no sensitivity to seasonal variations to incoming solar radiation (5). The effect of atmospheric water vapor on the signal also is negligible and has no impact on the data quality (5, 7). We compared QSCAT data with other similar sensors, such as the TRMM precipitation radar (TRMM-PR) surface backscatter for the continuation of the data record to examine the changes in surface moisture during the 2010 drought. We found no other radar measurements with strong sensitivity to forest canopy characteristics (Fig. S1) (8).

We used QSCAT backscatter data (σ^0) at H polarization in ascending node from morning passes (0600 LST) to create both monthly and dry-season (JAS) anomalies for the entire time series using the equation

$$\sigma^0 \text{ anomaly}(i, j) = \frac{\sigma_y^0(i, j) - \langle \sigma_{1999-2009}^0(i, j) \rangle}{STD(\sigma_{1999-2009}^0(i, j))}$$

The H and V polarizations provided similar results. However, the morning passes showed stronger anomaly than the late afternoon passes, probably because of the higher canopy water content in the morning with trees naturally in the least-stressed condition because of overnight hydrological recharge (higher QSCAT backscatter) and hence greater sensitivity to the water content status of the canopy (5). Note that in all analyses, we used the QSCAT backscatter power values in linear scale (m^2/m^2) and not in decibels to allow compatible analysis between rainfall and QSCAT.

QSCAT Performance. QSCAT backscatter data (σ^0 in decibels) were collected on a sun-synchronous orbit with twice-daily swaths over a given point, providing morning passes (~ 0600 LST) in ascending orbits and evening passes (~ 1800 LST) on descending orbits. We acquired aggregated data covering July 1999 through November 2009 from the NASA Scatterometer Climate Record Pathfinder project. The data were reprocessed from the native sensor resolution of ~ 25 km, with roughly daily coverage, by combining multiple orbit passes to generate image products with improved spatial resolution (4.45 km) and reduced temporal resolution (4D) (9). The QSCAT backscatter data were calibrated throughout the instrument lifetime using in situ measurements and data from other sensors (9).

In November 2009, the QSCAT antenna ceased to spin after its continuous operation over more than a decade. However, the sensor continued to collect valid backscatter data over narrow tracks and at a fixed azimuth angle; these data are being used to calibrate and validate Oceansat, a new sensor with similar configuration from the Indian Space Agency. There has not been any evidence of QSCAT backscatter calibration failure or signal degradation during its operation for global coverage. QSCAT

has provided reliable data products of wind speed over oceans (10), soil moisture over land (11), and sea ice cover over polar regions (12). To demonstrate the stability of the QSCAT signal over land after the 2005 drought, we developed the backscatter anomaly over the northwest region of Amazonia that was not affected by the 2005 drought (Fig. S4). Similar patterns may be observed readily over other regions of the land and ocean.

Biophysical Information in QSCAT Backscatter. Space-borne scatterometers have provided continuous microwave coverage of the earth for approximately two decades. These scatterometers originally were designed to measure oceanic surface winds and land surface parameters such as soil moisture. However, their data also are extremely useful in a broad range of ice and land applications, including the use of extensive scatterometer time series to determine seasonal and interannual variability and possible relationships to climate change (9, 13). To date, there have been five space-borne scatterometers with long time-series measurements that have flown on different international spacecrafts. These include the SeaWinds scatterometer onboard QSCAT (13.4 GHz), which launched in 1999 and continued collecting data until November 2009; the 5.3-GHz scatterometer from the European Space Agency (ESA), carried onboard both the ERS-1 and ERS-2 satellites since 1991 and continuing as the ESA advanced scatterometer (ASCAT) since 2009 (9); and TRMM-PR, operating since its launch in 1997 at K_u band (14 GHz) and used primarily for rain measurements over the land surface and a non-sun-synchronous orbit (14, 15).

The scatterometer system transmits radar pulses and receives the backscatter energy from the surface with its intensity represented as the normalized radar backscatter coefficient (σ^0) (Fig. S1). The magnitude of σ^0 depends on the roughness and dielectric properties of the particular target under observation, indicating a strong sensitivity of σ^0 to the surface soil moisture over bare surfaces or open and low-density vegetation (e.g., grass, shrub lands) (13) and canopy structure and water content over densely covered vegetation (e.g., tropical rainforests) (8).

In this study, we chose to use QSCAT data over all other existing datasets to monitor changes of canopy properties over Amazonia for several reasons: (i) QSCAT provides one of the longest records of continuous measurement, with consistent calibration globally. Other sensors, such as the European remote-sensing satellite (ERS) series and ASCAT, provide measurement from three different spacecrafts, with potential differences in calibrations that may affect long-term time-series analyses. (ii) QSCAT measurements are performed at higher frequency (13.4 GHz) than ERS and ASCAT sensors (5.3 GHz), with less penetration into the forest canopy and relatively no impact of soil moisture on the backscatter in densely vegetated surfaces such as Amazonia. (iii) QSCAT observations are performed at high incidence angles (46° and 54° from zenith), suggesting a strong sensitivity to only the top few meters of forest canopy (Fig. S1). To date, there is clear evidence that QSCAT backscatter data can monitor forest canopy structure and water content with significant correlations to seasonal and spatial variations of the canopy leaf area index (LAI) in densely forested areas (8). It has been demonstrated that QSCAT time-series data can capture phenological variations over different biomes globally (16).

TRMM-PR measurements also have been collected continuously over a long period (1997 to present) at a relatively higher temporal frequency than QSCAT twice a day. TRMM-PR standard backscattered product PR-2A21 is the σ^0 value with a rain flag over the range of incidence angles that may be processed to eliminate data when it rains and to develop surface backscatter similar to QSCAT data. The TRMM-PR observations are performed at off-nadir angles (−17° to +17°) (17), making the backscatter measurements over Amazonia strongly influenced by the surface soil moisture and scattering from

understory vegetation visible to the scatterometer through canopy gaps (8).

The penetration depth of the Ku-band signal into the tropical forest canopy between the two sensors may be simulated using a simple water cloud model or forest canopy 3D models used for radar backscatter at different frequencies (18–21). The one-way attenuation can be simulated using the following model (21):

$$\tau = \exp[-\kappa \bullet G(\theta) \bullet V \bullet \varepsilon'' \bullet t / \cos(\theta)],$$

where $G(\theta)$ is the gap fraction seen at any incidence angle; V is a vegetation parameter such as the canopy water content, sometimes expressed as the LAI; κ is the adjusted Ku-band propagation constant into the canopy ($2\pi/\lambda$, λ :wavelength) (18, 19); ε'' is the complex part of the leaf dielectric constant related to its water content (6); and t represents the opacity of a single leaf adjusted by leaf thickness (20). Using a landscape-scale LAI = 6 for rainforest canopies (22) as V , varying the gap fraction seen at different incidence angles (23), we can simulate the attenuation and the half-power (when incidence energy of the microwave reaches its half-power) penetration depth (17) to examine the relative sensitivity of Ku-band backscatter to different layers of the forest canopy (Fig. S1). The overall variations of the penetration depth may be larger than what has been simulated because microwave signal propagates farther into the canopy than its half-power level, and at large footprints (5 km), there often are large gaps due to variations of forest cover.

In summary, factors affecting the QSCAT data are as follows: (i) There are seasonal changes in canopy water content that also may be related to phenology in temperate forests and seasonal tropical forests (18). (ii) Because of the wavelength of the radar signal (about 2.1 cm), the penetration depth, and the coarse resolution image characteristics, the water content and structure of branches and leaves affect the scattering as they form the upper-canopy roughness and dielectric properties. Leaf clumping, the orientation of scatterers, and other minor structural characteristics have less impact on the QSCAT radar backscatter. (iii) Structural changes of forest canopy, such as large-scale degradation and deforestation, that may change the canopy roughness, create gaps, and affect the water content or biomass of the forest canopy can change the backscatter signal. (iv) In our monthly time-series analysis, the impact of direct rain and morning dew or other short-term climate events is negligible. (v) Soil moisture effect is relatively small on the QSCAT data, except in areas where the forest cover is patchy and there are large areas of exposed soil within the QSCAT pixel.

Results from the TRMM-PR analysis over the Amazon basin show a similar and strong dependence of incidence angle on radar backscatter, causing 16–18-dB differences in backscatter from a 0° to 5° incidence angle (16). In general, the TRMM-PR data processed with elimination of the signal during the rain event may carry information about the surface moisture smoothed over time without showing the rain events (14). We used the TRMM-PR data and developed the backscatter anomaly over all of Amazonia to demonstrate the strong anomaly for the 2005 and 2010 droughts (Fig. S11). Although both datasets show similar regions for the 2005 drought in Amazonia, the QSCAT signal is much stronger and widespread as it shows only the changes in the canopy properties and has relatively no information from the soil moisture. The 2010 backscatter anomaly shows the widespread changes in surface moisture over Amazonia extending from the early part of the year and continuing through the end of 2010. The overall behavior of the TRMM-PR anomaly closely follows the rainfall anomaly shown in Fig. 2 without the strong signal of rain events, suggesting that the backscatter is responding to the surface moisture (representing soil and canopy moisture) rather than the upper-canopy moisture and structure change.

Time-Series Analysis. We used the QSCAT backscatter values from January 2000 to December 2009 (repeating the November value for the missing December measurements) to create a complete 10-y (120-mo) time series for the analysis. We applied an autoregressive moving-average (ARMA) model to analyze the QSCAT time-series anomaly. ARMA is based on the autoregressive (AR) model that represents the current value of a process by a function of previous values, plus some noise:

$$X_t = k + \sum_{i=1}^p \phi_i X_{t-i} + \varepsilon_t,$$

where k is a constant, ε_t is a white noise with zero mean and constant variance, and ϕ_1, \dots, ϕ_p are the parameters of the model. The order of AR (p) process is defined by the time lag of the time-series process p using an autocorrelation function (ACF). Once the order of the model is defined, the parameters are estimated using a least-squares regression approach. The time series would follow a moving-average AR process if we found that the present observation depended less on the previous observation and more on how the previous value differed from its average value (24). The order of the AR model is defined using ACF or partial ACF (PACF) functions, with autocorrelation with lag- p defined as:

$$\rho_p = \frac{\sum_{t=1}^{N-p} (X_t - \bar{X})(X_{t+p} - \bar{X})}{\sum_{t=1}^N (X_t - \bar{X})^2};$$

with SE: $SE_p = \sqrt{(1 + 2 \sum_{i=1}^{p-1} \rho_i^2)/N}$.

The SE is used to test the significance of the lag time and to approximate the confidence bounds on the estimate. The PACF is the same as the ACF when any linear dependence in the time-series observations is removed. We use a combination of programs developed in Interactive Data Language (IDL) and R (programming language) to perform the analysis.

We used the BFAST (Breaks in Additive Season and Trend) algorithm developed in R (<http://bfast.R-Forge.R-project.org/>). The algorithm is based on an additive decomposition model that iteratively fits a piecewise linear trend and seasonal model to the data (25):

$$X_t = T_t + S_t + R_t, \quad t = 1, \dots, N,$$

where X_t is the observation data at time t and T_t , S_t , and R_t are, respectively, the trend, seasonal, and remainder variation components of the data. The algorithm assumes that T_t is piecewise linear with potential breakpoints that can be determined by fitting the linear models iteratively to different sections of the data in a moving window. The abrupt changes are detected by minimizing the residual sum of squares, and their optimal positions in time series can be determined based on the Bayesian information criterion (25).

Spatial Analysis. We used the QSCAT monthly anomalies representing the changes in canopy properties and TRMM monthly water deficit anomaly (WDA) representing the drought intensity to examine how the two are related and change across landscape and time. To examine the relationship between the two, we developed a spatiotemporal cross-correlation analysis between QSCAT and TRMM anomalies by resampling the QSCAT data to match the TRMM pixel and performing pixel-by-pixel correlation. We calculated the Pearson correlation coefficient between the ranks of variables on a pixel-to-pixel basis using

$$r = \frac{\sum_i (x_i - \bar{x})(y_i - \bar{y})}{\sqrt{\sum_i (x_i - \bar{x})^2 \sum_i (y_i - \bar{y})^2}},$$

where r is known as the Spearman rho between ranked variables x_i and y_i at a pixel location, with \bar{x} and \bar{y} being the average of variables over the time interval. In this case, x_i and y_i are the QSCAT and TRMM anomalies over the period 2000–2009. The correlation coefficients that are significantly different from zero are then shown for each pixel. We performed the correlation with time lags extending up to 18 mo (15% of the total points in the time series) in both directions.

Over southwestern Amazonia, the post-2005 backscatter values and monthly anomalies stayed lower relative to the pre-2005 values, as shown in Fig. 2. We calculated the average QSCAT monthly anomalies for all pixels within a TRMM pixel (0.25°) and computed the difference between QSCAT anomaly (less than -1.0σ) and TRMM WDA. The negative difference in normalized anomaly suggests a lag in recovery of QSCAT anomaly relative to TRMM WDA. We mapped the spatial distribution of changes in pixels that were affected by the 2005 drought using the slope of the QSCAT – TRMM WDA monthly anomaly at each pixel from September 2005 to November 2009. Pixels with significantly ($P < 0.01$) larger negative slopes represent areas with a longer lag in QSCAT backscatter recovery. The map was colored based on the negative slope of difference over the time series since the 2005 drought. The spatial analysis also was performed on the QSCAT data to quantify the average amplitude of backscatter seasonality over the entire QSCAT time series (2000–2009) to identify areas with the greatest seasonality in canopy water content (Fig. 4B).

Impact of Deforestation and Fire. Time-series analysis of the QSCAT data and the persistent post-2005 negative anomaly may be affected by the annual deforestations occurring particularly in the southern and southwestern regions of Amazonia. We included three datasets to remove the effect of nonforest land cover types and deforestation from the analysis of the QSCAT data. First, we used the Moderate Resolution Imaging Spectroradiometer (MODIS) level 3 global 0.05° Land Cover Type Yearly Climate Modeling Grid product (MCD12C1, V051) for the year 2005 to identify the forested areas and mask out nonforested vegetation including deforested landscapes classified as pasture and crops (<https://lpdaac.usgs.gov/products/>). Forest areas were identified using five main forest classes in the MODIS land cover map: evergreen needleleaf forest, evergreen broadleaf forest, deciduous needleleaf forest, deciduous broadleaf forest, and mixed forests.

Second, we included the MODIS Vegetation Continuous Fields (VCF) product (<http://glcf.umiaccs.umd.edu/data/vcf/>) produced at 500-m resolution annually (2001–2005). We used the 2005 VCF product, aggregated it to the QSCAT resolution of 0.05°, and developed a forest cover mask by eliminating all pixels $<50\%$ of tree cover. We applied the masks generated from the MODIS land cover data and VCF to exclude all nonforested pixels from the QSCAT backscatter anomaly analysis.

We also used the European Space Agency's (ESA) GlobCover 2009 land cover data at 300-m resolution produced by ESA 2010 and Université Catholique de Louvain. The map was derived from Envisat's Medium Resolution Imaging Spectrometer (MERIS) data and was used to mask all potential pixels representing the nonforest types before the end of 2009 (www.esa.int/esaCP/SEM5N3TRJHG_index_1.html). The GlobCover forest mask was produced at 300-m resolution using all forest cover types and later was resampled to 0.05°, and all pure pixels of forest masks were used as a new mask in the QSCAT anomaly analysis. In general, the GlobCover 2009 data might have been

the only mask to eliminate the deforested pixel from our analysis. However, using the three masks in our analysis ensures that all deforestations occurring from 2000 to the end of 2009 are completely eliminated from the anomaly analysis and any observed variations in QSCAT data are directly related to changes in canopy properties in the more intact forests.

The effect of fire has been quantified using the active fire product derived from monthly accumulated data, from January 2001 to December 2010, at 1-km spatial resolution, from MODIS–Terra sensor product MCD14ML collection 5. This product detects flaming and smoldering fires approximately 1 km² in size under cloud-free conditions; for particularly “good” observational conditions (near-nadir and reduced smoke), flaming fires of 100 m² can be detected (26). Underestimation of fire detection may occur in situations in which the fire has started and ended between the satellite overpasses, in cloudy conditions, or under the forest canopy, or when it is too small or too cool for the 1-km² footprint (26). We used only high-confidence fire pixels for processing the data, allowing a >80% confidence level in detecting fires. The monthly fire pixel count was then aggregated at 0.1° spatial resolution. Pre-2005 drought fire effects were masked by summing the monthly data from January 2001 to June 2005, when the breakpoint in QSCAT data due to the 2005 drought occurred. The post-2005 drought effects were masked by summing the number of fires from June 2005 to December 2009. We also

computed the accumulated number of fires in 2010 to examine what percentage of the pixels affected by the 2005 drought and having persistent effects on canopy structure and water content was susceptible to future fires.

Climate Analysis. We extended the analysis of rainfall over the southwestern and entire Amazon basin by including the long-term monthly data from the Climatic Research Unit (CRU; www.cru.uea.ac.uk/; 1930–2005). We computed the DWDA from CRU and combined it with TRMM (1998–2010) to show the long-term variations in precipitation anomalies over the Amazon basin (Fig. S9). We developed spatial correlation between TRMM (1998–2010) and CRU (1970–2009) monthly anomalies and the two climate indices: the Tropical North Atlantic Index (TNA) and the Southern Oscillation Index (SOI; downloaded from www.esrl.noaa.gov/psd/data/timeseries/). These indices represent, respectively, the fluctuation in sea surface temperature in the tropical North Atlantic and the difference between sea level pressures in the Pacific Ocean (at Tahiti, Darwin, and Australia) (27, 28). The correlations are performed on a pixel-to-pixel basis for the entire region using the Spearman rank correlation method (above). The TRMM WDA over southwestern Amazonia and TNA index were plotted together to demonstrate the clear out-of-phase behavior of rainfall patterns with TNA in the region (Fig. S10).

- Shuttleworth WJ (1989) Micrometeorology of temperate and tropical forest. *Philos Trans R Soc London Ser B* 324:299–334.
- Aragão LEOC, et al. (2007) Spatial patterns and fire response of recent Amazonian droughts. *Geophys Res Lett* 34:L07701–GL028946.
- Dracup JA, Lee KS, Paulson EG, Jr. (1980) On the definition of droughts. *Water Resources Research* 16(2):297–302.
- Asner GP, Alencar A (2010) Drought impacts on the Amazon forest: The remote sensing perspective. *New Phytol* 187(3):569–578.
- Frolking S, et al. (2010) Tropical forest backscatter anomaly evident in SeaWinds scatterometer morning overpass data during 2005 drought in Amazonia. *Remote Sens Environ* 115:897–907.
- Ulaby FT, Moore RK, Fung AK (1986) *Microwave Remote Sensing—Active and Passive* (Artech House, Norwood, MA), Vol III.
- Slik JW (2004) El Niño droughts and their effects on tree species composition and diversity in tropical rain forests. *Oecologia* 141(1):114–120.
- Frolking S, et al. (2006) Evaluation of the SeaWinds scatterometer for regional monitoring of vegetation phenology. *J Geophys Res* 111:D17302.
- Long DG, Drinkwater M, Holt B, Saatchi S, Bertoia C (2001) Global ice and land climate studies using scatterometer image data. *Eos Trans AGU* 82(43):503.
- Ricciardulli L, Wentz F (2011) *Reprocessed QuikSCAT (V04) Wind Vectors with Ku-2011 Geophysical Model Function* (Remote Sensing Systems, Santa Rosa, CA), Remote Sensing Systems Tech Rep 043011.
- Nghiem SV (2012) Microwave remote sensing of soil moisture—science and applications. *Remote Sensing of Drought: Innovative Monitoring Approaches*, eds Wardlow BD, Anderson MA, Verdin JP (CRC, Boca Raton, FL).
- Bartsch A (2012) Ten years of seawinds on QuikSCAT for snow applications. *Remote Sens* 2:1142–1156.
- Kimball JS, McDonald KC, Keyser AR, Frolking S, Running SW (2001) Application of the NASA scatterometer (NSCAT) for determining the daily frozen and nonfrozen landscape of Alaska. *Remote Sens Environ* 75:113–126.
- Wagner W, Scipal K (2000) Variability in ERS scatterometer measurements over land. *IEEE Trans Geosci Rem Sens* 38(4):1777–1782.
- Frison PL, Mougín E (1996) Monitoring global vegetation dynamics with ERS-1 wind scatterometer data. *Int J Remote Sens* 17(16):3201–3218.
- Satake M, Hanado H (2004) Diurnal change of Amazon rain forest σ^0 observed by Ku-band spaceborne radar. *IEEE Trans Geosci Rem Sens* 42(6):1127–1134.
- Kawanishi T, et al. (2000) TRMM precipitation radar. *Adv Space Res* 25:969–972.
- Moran MS, Vidal A, Troufleau D, Inoue Y, Mitchell TA (1998) Ku- and C-band SAR for discriminating agricultural crop and soil conditions. *IEEE Trans Geosci Rem Sens* 36:265–272.
- Attema EPW, Ulaby FT (1978) Vegetation modeled as a water cloud. *Radio Sci* 13(2):357–364.
- Saatchi S, Mughaddam M (2000) Estimation of crown and stem water content and biomass of boreal forest using polarimetric SAR imagery. *IEEE Trans Geosci Rem Sens* 38:697–709.
- Schneebeil M, et al. (2011) Relating X-band opacity of a tropical tree canopy to sapflow, rain interception, and dew formation. *Remote Sens Environ* 115(8):2116–2125.
- Clark DB, Olivás PC, Oberbauer SF, Clark DA, Ryan MG (2008) First direct landscape-scale measurement of tropical rain forest Leaf Area Index, a key driver of global primary productivity. *Ecol Lett* 11(2):163–172.
- Canham CD, et al. (1990) Light regimes beneath closed canopies in temperate and tropical forests. *Can J For Res* 20:620–631.
- Hamilton J (1994) *Time Series Analysis* (Princeton Univ Press, Princeton, NJ).
- Pires JM, Prance GT (1985) The vegetation types of the Brazilian Amazon. *Key Environments: Amazonia*, eds Prance GT, Lovejoy TE (Pergamon, New York), pp 109–145.
- Giglio L (2010) *MODIS Collection 5 Active Fire Product User's Guide, Version 2.4* (Science Systems and Applications, Inc., University of Maryland, Department of Geography).
- Enfield DB, et al. (2001) The Atlantic Multidecadal Oscillation and its relation to rainfall and river flows in the continental U.S. *Geophys Res Lett* 28:2077–2080.
- Malhi Y, Wright J (2004) Spatial patterns and recent trends in the climate of tropical rainforest regions. *Philos Trans R Soc Lond B Biol Sci* 359(1443):311–329.

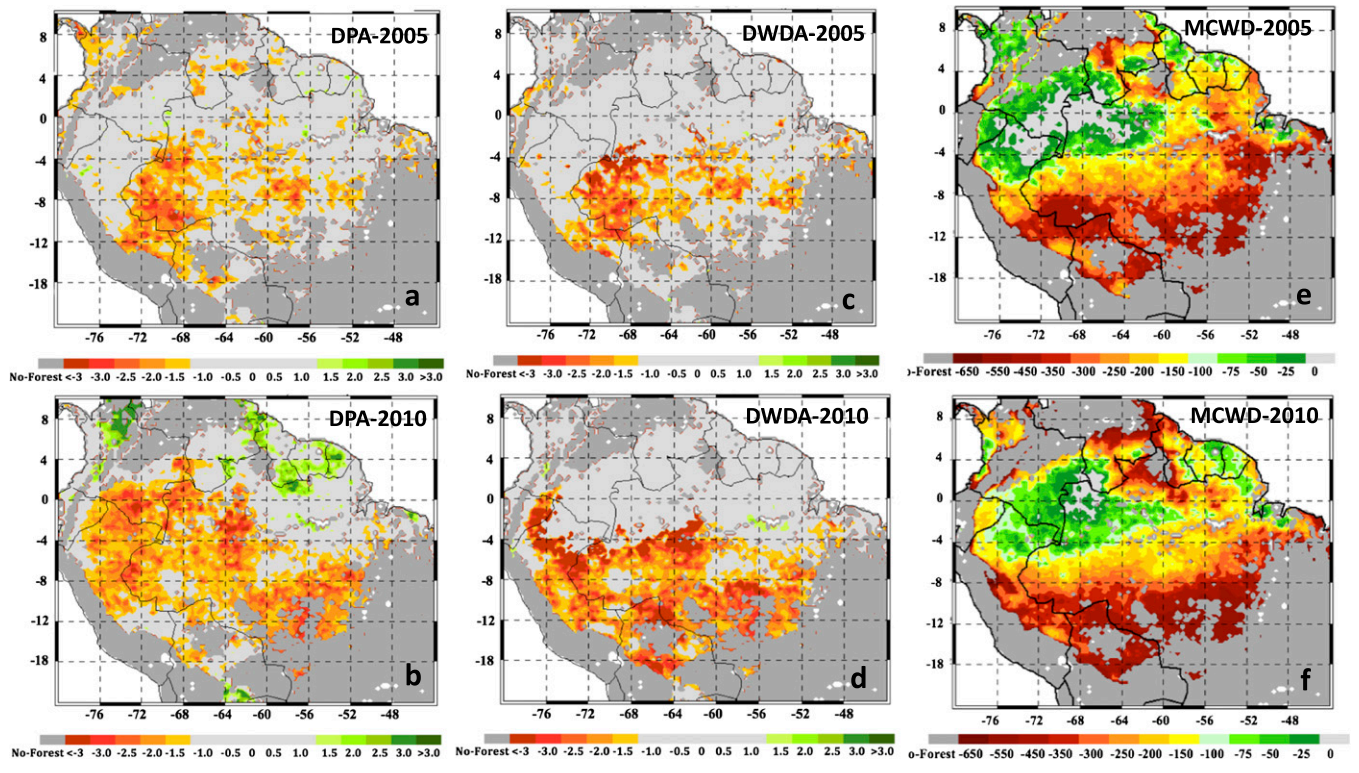


Fig. S2. Spatial extent and severity of the Amazonian droughts in 2005 and 2010 using standardized DPA (A and B), DWDA (C and D), and MCWD (E and F), derived from TRMM monthly precipitation data.

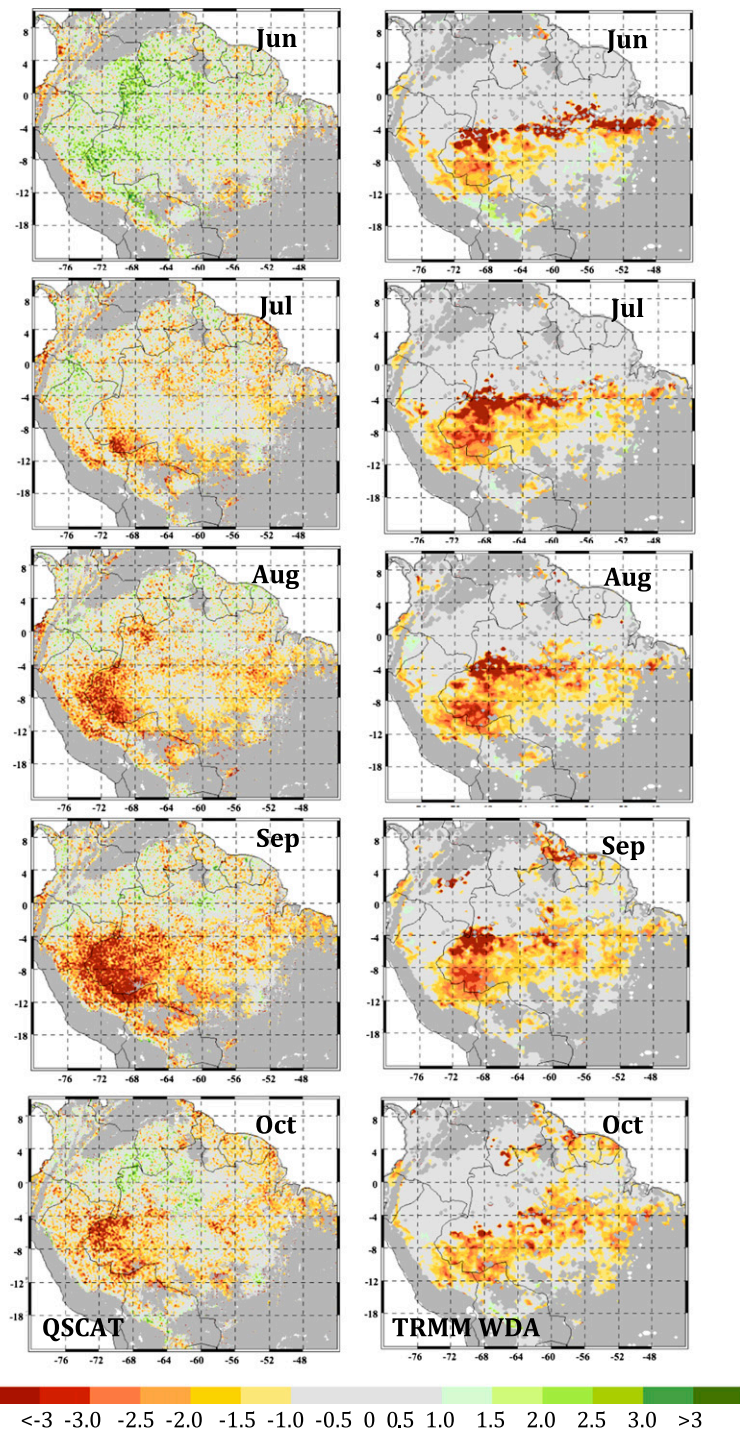


Fig. S3. Monthly changes in DWDA along with the evolution of monthly QSCAT dry-season (JAS) anomaly, indicating the gradual development of water stress in the southwestern region of Amazonia in 2005 and the changes in canopy properties (e.g., water content) in response to the water stress. The QSCAT response to water deficit in Amazonia appears with almost 1-mo lag.

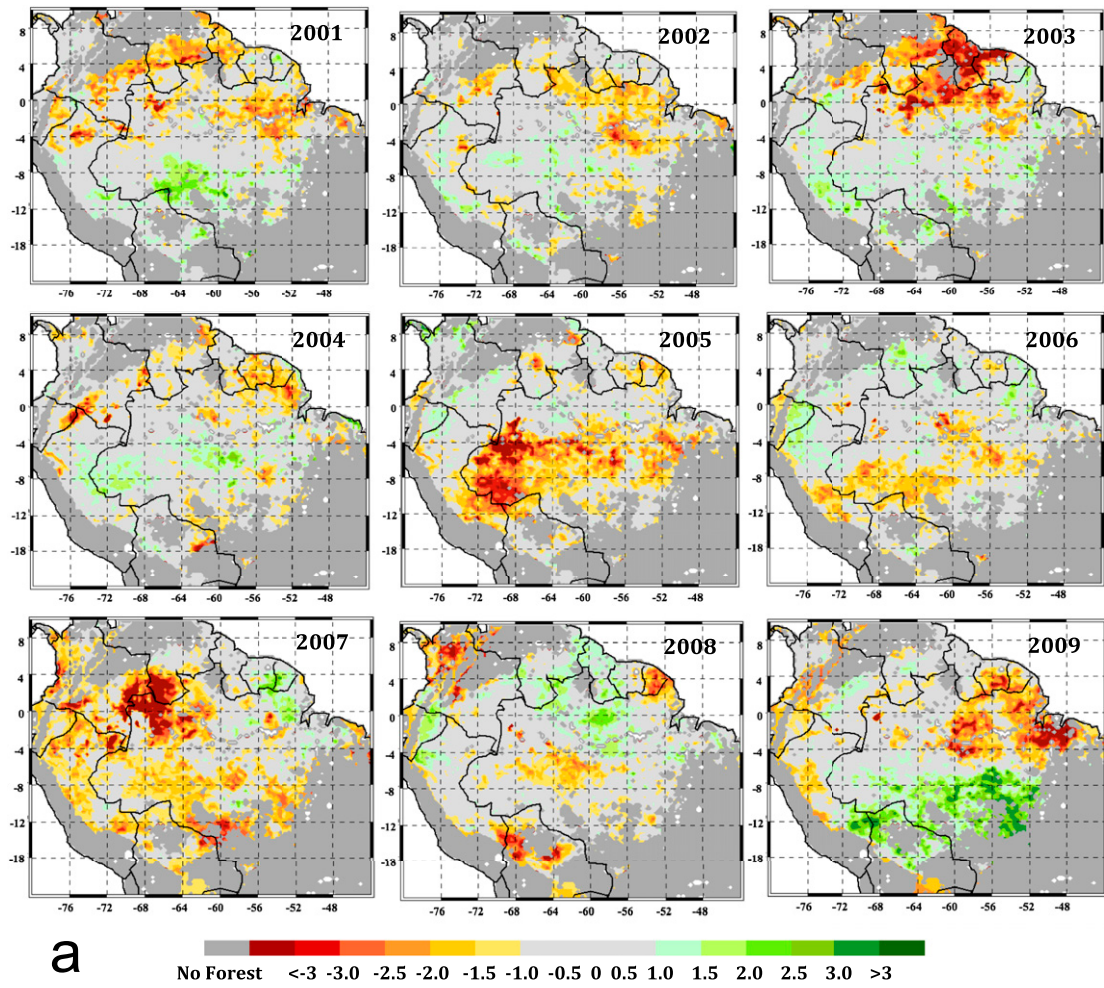


Fig. S4. (Continued)

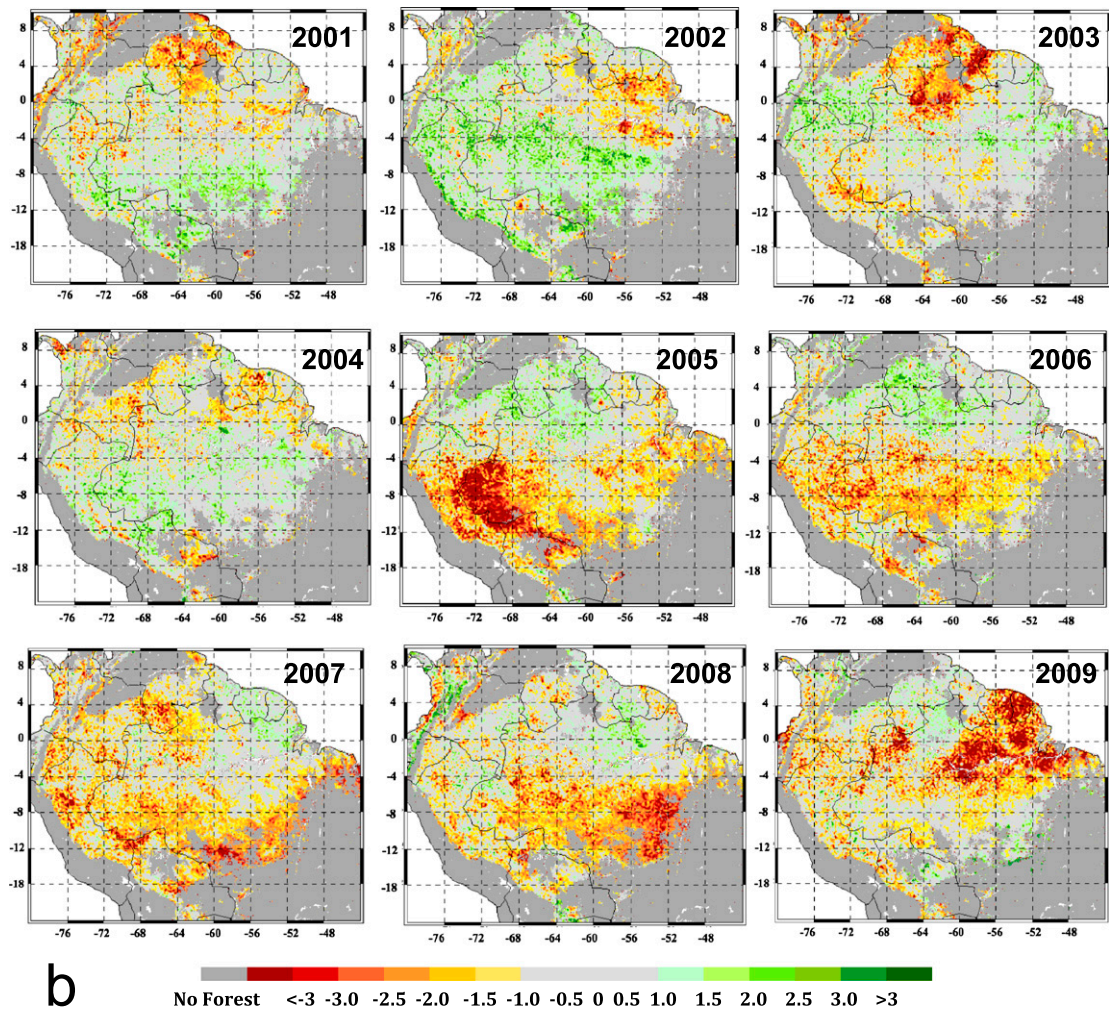


Fig. 54. The distribution of normalized anomalies of pixels within the western Amazonia window. Shown here are the DWDA from TRMM (A) and the QSCAT backscatter power (B). Annual DWDA from TRMM (A) and the corresponding changes in canopy properties are captured by the annual dry-season (JAS) anomaly of QSCAT backscatter data (B) over the last decade (2001–2009). Normalized anomaly is colored beyond $\pm 1.0 \sigma$, showing only pixels with significant departure from long-term average. QSCAT negative anomaly persists over the south and western regions of Amazonia after the 2005 drought through 2009, when a strong positive anomaly of rainfall makes the QSCAT anomaly less significant. The 2007 moderate drought also enhanced the QSCAT negative anomaly in 2007 and subsequently in 2008.

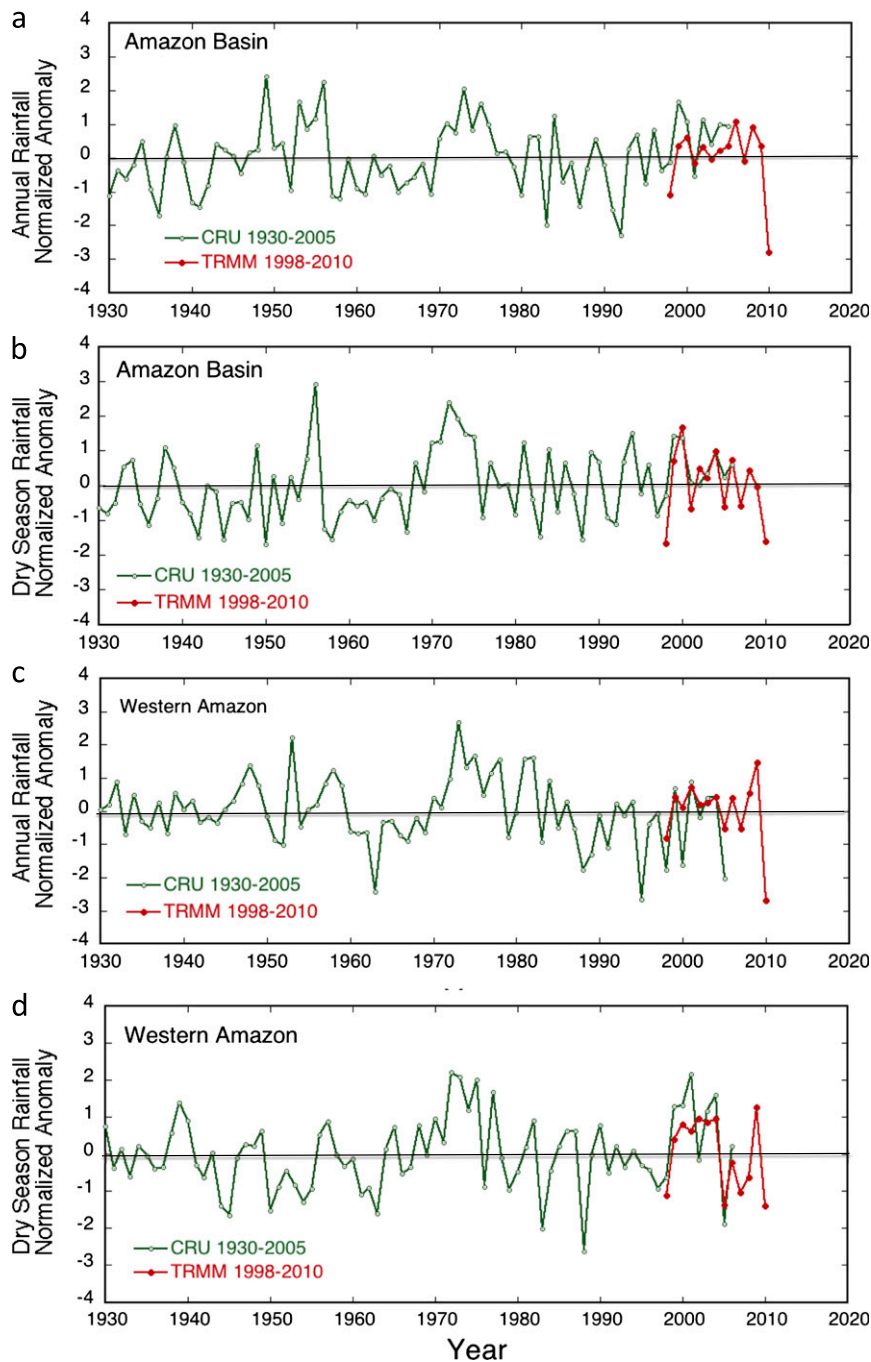
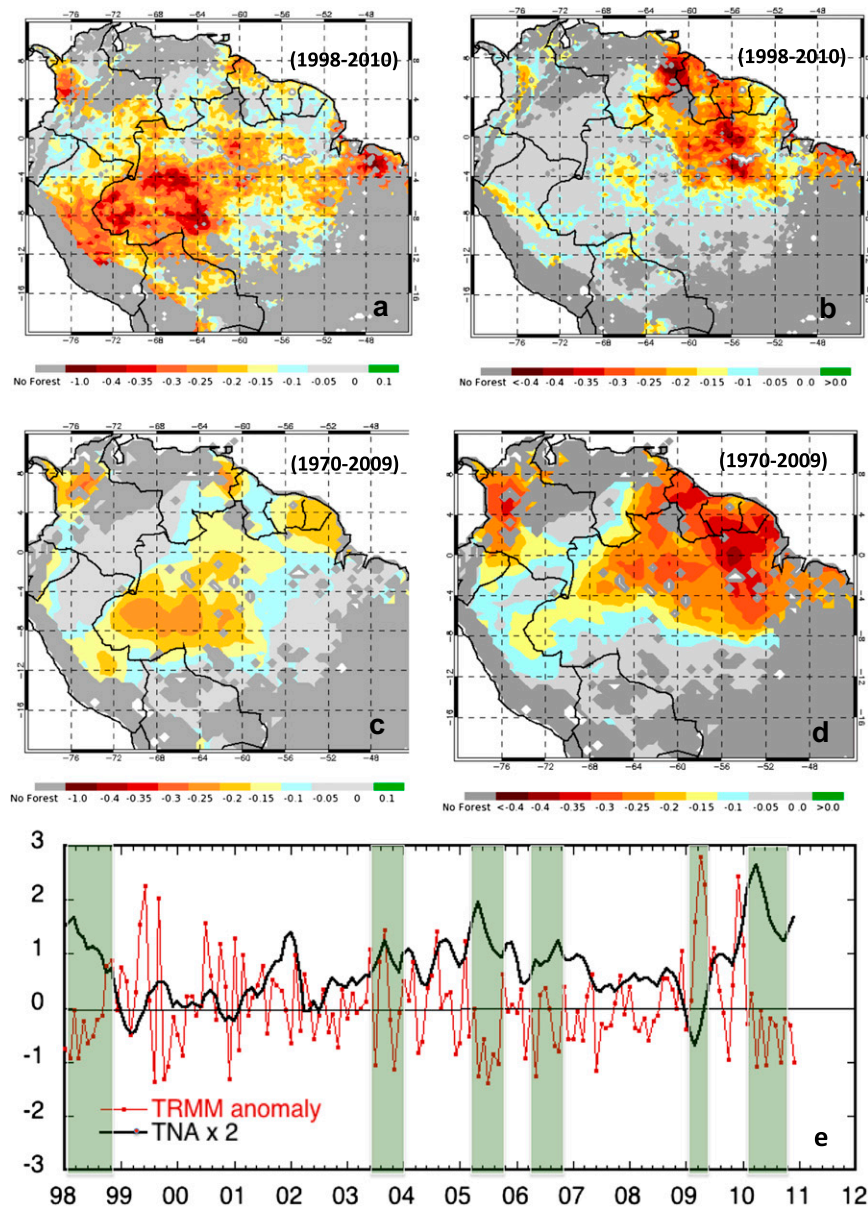


Fig. S9. Long-term time series (1930–2010) of rainfall anomaly over the entire Amazon basin and southwestern region (window: 4°S – 12°S , 76°W – 66°W) derived from CRU (1930–2005) and TRMM (1998–2010). Because of potential differences in absolute value of rainfall, the anomalies were calculated separately for each dataset. Over the past 30 y, starting from the mid-1970s and early 1980s, we observe a clear decline in annual rainfall anomaly over southwestern Amazonia, with larger variations and stronger negative anomalies over the entire Amazon basin. This feature agrees with the long-term modes of climate variability (24–28 y) (1) and shorter oscillations (4–6 y) (2). The number of negative anomalies significantly greater than -1.0 standard deviation (SD) increased in the past 30 years (1980–2010) compared with the previous 50 y (1930–1980) by a factor of two. The panels show the annual rainfall (A) and the dry season (B) rainfall normalized anomaly over the entire Amazon basin, and similar time series anomaly for annual (C) and dry season (D) of the western Amazonia.

1. Marengo JA, et al. (2008) The drought of Amazonia in 2005. *Journal of Climate* 21:495.

2. Marengo JA, et al. (2011) The drought of 2010 in the context of historical droughts in the Amazon region. *Geophys Res Lett* 38:L12703.



Time Series (1998-2010)

Fig. S10. Spatial correlation of TNA (A) and SOI (B) indices with the TRMM (1998–2010) and CRU (1970–2009) monthly rainfall anomalies over the Amazon basin. Areas of western Amazonia affected by recent droughts showed significant Pearson correlation with (A) a high TNA index over the past decade (1998–2010: $r > 0.55$, $P < 0.001$, ± 1 -mo lag) and (C) over the past 40 years using the CRU data (1970–2009, $r > 0.38$, $P < 0.01$, ± 1 -mo lag). Whereas El Niño events represented by SOI showed only significant correlation with monthly (B) TRMM precipitation anomalies in northeastern Amazonia ($r > 0.43$, $P < 0.005$, ± 1 -mo lag) and (D) the monthly CRU data ($r > 0.41$, $P < 0.005$, ± 1 -mo lag) with higher average rainfall during the dry season and less probability of droughts. The geographical regions of TNA-related droughts are in the south and southwestern margins of Amazonia. Monthly WDAs derived from TRMM (1998–2010) when plotted against the TNA index showed an out-of-phase behavior, with low rainfall corresponding to a higher TNA index (E). The TNA index is multiplied by 2 to better demonstrate the out-of-phase relationship to the TRMM anomalies on the same graph.

